Investigation of Unbalanced Magnetic Force in Permanent Magnet Brushless DC Machines with Diametrically Asymmetric Winding

M. Jafarboland [*], *S. M. Mousavi*

Department of Electroceramics and Electrical Engineering, University of Malek-Ashtar, Iran

Abstract- *The purpose of this paper is calculation of Unbalanced Magnetic Force (UMF) in permanent magnet brushless DC (PMBLDC) machines with diametrically asymmetric winding and investigation of UMF variations in the presence of phase advance angle. This paper presents an analytical model of UMF in surface mounted PMBLDC machines that have a fractional ratio of slot number to pole number. This model is according to a 2-D analytical field model. By an appropriate choice for slot number to pole number ratio, the magnitude of UMF is zero and this is achieved only when the stator slot and coils distribution is symmetrical about diameter of machine. The presented model is validated by 2-D finite element analysis and a good agreement is obtained between them. Also, UMF is calculated in the presence of different phase advance angles. UMF was calculated for 33-slot/34-pole and 36-slot/34-pole external rotor machines with analytical and finite element method. Machine with 33-slot/34-pole has significantly larger UMF than 36-slot/34-pole machine. Also UMF is calculated for 33-slot/34-pole machine in the presence of phase advanced angles and results show that the magnitude of UMF changes with the amount of phase advance angle periodically. The impact of phase advance angle method on the magnitude of UMF is investigated for the first time by finite element method. Due to increasing or decreasing of the magnitude of UMF in the presence of different phase advance angles, the magnitude of UMF is an important feature in the selection of appropriate phase advance angle.*

Keyword: Asymmetric winding, Phase advance angle, Permanent magnet Brushless DC machines, Pole and slot number combination, Unbalanced magnetic force.

1. INTRODUCTION

Electrical machines use 70 to 75 percent of the total electricity which is consumed in industry [1]. PMBLDC machines with fractional ratio of slot number to pole number are very popular due to their advantages such as high efficiency and torque density [2, 3], low cogging torque [4, 5], high flux weakening capability [6], short end winding [7-13] and etc. Nonetheless they have the problem of noise and vibration in their structures that reduce the bearings lifetime [14]. In permanent magnet machines there are noise and vibration due to cogging torque and UMF. Cogging torque is a pulsating torque caused by changing permeance between permanent magnets and stator slots. Many ways have been developed to minimize the cogging torque [15].

Since UMFs have more contribution than cogging torque in generation of noise and vibration, this paper

focuses on calculating them. In general, factors which generate UMFs are static/dynamic rotor eccentricity, stator eccentricity, imperfect magnetization and diametrically asymmetric windings. The UMF due to stator eccentricity and static/dynamic rotor eccentricity was investigated in permanent magnet brushless machines [16-18]. Eccentricity fault causes UMF which results in vibration and acoustic noise [19]. In [20], Influence of imperfect magnetization in permanent magnet machines was investigated. Researchers in [21] have showed that UMFs exist in PMBLDC machines even when there are no eccentricities. This is due to asymmetry in stator slot and coils. Among different combinations of slot/pole number, machines with $2p = N_s + 1$ and $2p = N_s + 2$ (p equals to pole pairs and N_s is stator slot number) are very desirable because of having coil pitch close to pole pitch and consequent maximum flux linkage and high torque density [22, 23]. Some of these slot/pole number combinations produce UMF and it is very important that we would be able to recognize them before machine manufacturing. Many papers have investigated 3-slot/2-pole, 9-slot/8-pole, 9-slot/10-pole machines but in this paper machines with 33-slot/34-pole and 36-slot/34-pole were analyzed which received less attention and are being used in electrical

vehicles. Generally, a BLDC machine has two operation regions: constant torque operation and constant power operation [24]. At low speeds (constant torque operation), it is possible to ignore the coil inductance but at high speeds (constant power operation), the effect of coil inductance is very significant and the performance of machine is deteriorated. To solve this problem, there are many methods one of which is phase advance angle method [25]. In order to investigate the effect of the phase advance angle on the magnitude of UMFs, in this study UMFs are obtained in presence of various angles. In this paper, a 2-D analytical model for computation of flux densities of permanent magnet and armature reaction fields in PMBLDC machines will be presented then corresponding UMFs will be calculated based on Maxwell stress tensor method. Secondly machines will be simulated in Finite element software and flux densities and UMFs will be obtained from finite element method. The results from two methods (analytical and finite element) are compared and a good agreement was achieved between them. Also, UMFs have been calculated in presence of various phase advance angles in 33-slot/34-pole PMBLDC machine.

2.   PROTOTYPE MACHINES

Although the analytical model is capable of being implemented for any PMBLDC machine, in this research we have studied machines with 33-slot/34-pole and 36-slot/34-pole. Parameters for the two machines are shown in Table 1.

3.   ANALYTICAL MODEL

In this section the following assumptions were applied.
- The relative permeability of iron is infinite.
- The field is two dimensional.
- The end effect is negligible.
- Magnetic saturation, eddy current and hysteresis losses are ignored.

3.1. Permanent magnet field

The analytical expressions of the radial and tangential field components produced by the PMs on the open circuit in the air gap of slotless surface-mounted PM machines can be given by the following [26, 27]:

$$B_{mr}(r,\theta) = \sum_{n=1,3,5,...}^{\infty} K_B(n) f_{Br}(r)\cos(np\theta) \tag{1}$$

$$B_{m\alpha}(r,\theta) = \sum_{n=1,3,5,...}^{\infty} K_B(n) f_{B\theta}(r)\sin(np\theta) \tag{2}$$

$$K_B(n) = -\mu_0 M_{rm}\mu_r^{-1} np\left((np)^2 - 1\right)^{-1}$$
$$\cdot \frac{(A_{3n}-1)(R_m/R_r)^{2np} + 2(R_m/R_r)^{np-1} - (A_{3n}+1)}{\frac{(\mu_r+1)}{\mu_r}\left[1 - \left(\frac{R_s}{R_r}\right)^{2np}\right] - \frac{\mu_r-1}{\mu_r}\left[\left(\frac{R_s}{R_m}\right)^{2np} - \left(\frac{R_m}{R_r}\right)^{2np}\right]} \tag{3}$$

$$M_{rm} = 2B_r\mu_0^{-1}\alpha_p\left(\sin(np\alpha_p/2)/(np\alpha_p/2)\right) \tag{4}$$

$$f_{Br}(r) = (r/R_m)^{np-1} + (R_s/R_m)^{np-1}(R_s/r)^{np+1} \tag{5}$$

$$f_{B\theta}(r) = -(r/R_m)^{np-1} + (R_s/R_m)^{np-1}(R_s/r)^{np+1} \tag{6}$$

$$A_{3n} = np \tag{7}$$

The dimension of R_s , R_m and R_r are defined in Fig. 1. P is the pole pair number, α_p is the magnet pole-arc to pole-pitch ratio and b_o is the slot opening.

Table 1. The parameters of used machines

Parameter	33-slot/34-pole	36-slot/34-pole
Rated voltage (v)	72 v	
Rated power (p)	5000 w	
Rated speed (ω_r)	572 rpm	
Phase number (N_m)	3	
Air-gap length (g)	1.6 mm	
Motor active length (l_a)	54 mm	
Stator slot opening (b_o)	4 mm	
Magnet thickness (h_m)	5 mm	
Magnet remanence (B_r)	1.28	
Relative recoil permeability (μ_r)	1.05	
Magnet pole-arc to pole-pitch ratio (α_p)	0.8616	
Stator outer diameter $(2R_s)$	248 mm	
Rotor inner diameter $(2R_m)$	251.2 mm	
Rotor outer diameter $(2R_r)$	261.2 mm	
Winding turns per phase (W)	44	42
Magnet magnetization	Radial	

The influence of the stator slotting can be calculated by introducing a complex relative air-gap permeance based on the simplification of the actual slot shape beingreplaced by an ideal parallel slot [28]:

$$\tilde{\lambda}(\alpha,r) = \sum_\mu \tilde{\Lambda}_\mu \cos\mu N_s(\alpha + \alpha_{sa}) \tag{8}$$

$$\tilde{\Lambda}_\mu(r) = -\beta(r)(4/\pi)\left[0.5 + \frac{(\mu b_o/\tau_t)^2}{0.78125 - 2(\mu b_o/\tau_t)^2}\right]$$
$$\times \sin(1.6\pi\mu b_o/\tau_t) \tag{9}$$

$$\tau_t = 2\pi R_s / N_s \tag{10}$$

$$\beta(r) = 0.5\left[1 - \left(1\bigg/\sqrt{1 + (b_o/2g')^2(1 + v^2)}\right)\right] \tag{11}$$

$$y\pi b_o^{-1} = 0.5\ln\left[\left(\sqrt{a^2 + v^2} + v\right)\bigg/\left(\sqrt{a^2 + v^2} - v\right)\right] \\ + 2g'b_o^{-1}\arctan\left(2vg'\bigg/b_o\sqrt{a^2 + v^2}\right) \tag{12}$$

$$y = R_s + g' - r \tag{13}$$

$$g' = g + (h_m/\mu_r) \tag{14}$$

$$a^2 = 1 + (2g'/b_o)^2 \tag{15}$$

$$\alpha_{sa} = \pi/N_s \tag{16}$$
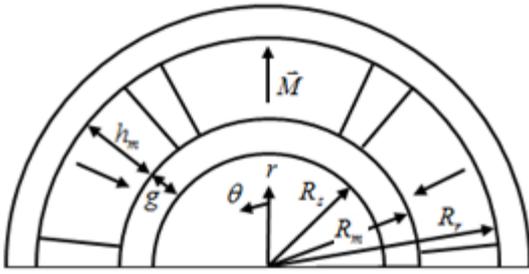
Fig. 1. Motor topologies.

Air-gap flux densities of permanent magnet field while considering the effect of stator slots in the air-gap can be expressed by Eqs. (17) and (18) [26, 29].

$$B_{mr,s}(r,\theta) = B_{mr}(r,\theta)\times\tilde{\lambda}(\alpha,r) \\ = \sum_{n=1,2,3,\dots}^{\infty} K_B(n)f_{Br}(r)\cos(np\theta)\times\tilde{\lambda}(\alpha,r) \tag{17}$$

For radial component and

$$B_{ma,s}(r,\theta) = B_{ma}(r,\theta)\times\tilde{\lambda}(\alpha,r) \\ = \sum_{n=1,2,3,\dots}^{\infty} K_B(n)f_{B\theta}(r)\sin(np\theta)\times\tilde{\lambda}(\alpha,r) \tag{18}$$

For tangential component. In Eqs. (17) and (18) $\theta = \alpha - \omega_r t$ that θ is the rotor angular position with respect to the axis of a magnet pole, θ is the stator angular position with respect to the axis of phase A winding and ω_r equals to mechanical angular velocity.

3.2. Armature reaction field

Radial and tangential air-gap flux densities of armature reaction field while considering the effect of stator slots in the air-gap can be expressed by Eqs. (19) and (20) [30].

$$B_{ar,s}(r,\alpha,t) = B_{ar}(r,\alpha,t)\times\tilde{\lambda}(\alpha,r) \\ = (3\mu_0 W/p\delta)\sum_{v=1}^{\infty}K_{sov}K_{dpv}F_v(r) \\ \cdot[i_a\sin v(\alpha) + i_b\sin v(\alpha + (2\pi/3)) + i_c\sin v(\alpha + (4\pi/3))] \\ \cdot\tilde{\lambda}(\alpha,r) \tag{19}$$

$$B_{a\alpha,s}(r,\alpha,t) = B_{a\alpha}(r,\alpha,t)\times\tilde{\lambda}(\alpha,r) \\ = (3\mu_0 W/p\delta)\sum_{v=1}^{\infty}K_{sov}K_{dpv}G_v(r) \\ \cdot[i_a\cos v(\alpha) + i_b\cos v(\alpha + (2\pi/3)) + i_c\cos v(\alpha + (4\pi/3))] \\ \cdot\tilde{\lambda}(\alpha,r) \tag{20}$$

In Eqs. (19) and (20), W is the number of series turns per phase, δ is difference between R_s and R_r ($\delta = |R_s - R_r|$), K_{sov} is slot opening factor and can be expressed as:

$$K_{sov} = (\sin(vb_o/2R_s))/(vb_o/2R_s) \tag{21}$$

In Eqs. (19) and (20) K_{dpv} is winding factor and its calculation method has been expressed in [31]. The winding factor is given by:

$$K_{dpv} = (8/n\pi)\sin(n\pi/33) \\ \cdot[(\cos(8n\pi/33) + \cos(4n\pi/33) + 0.5) - 0.25\sin(11n\pi/33)] \tag{22}$$

For 33-slot/34-pole BLDC motor and

$$K_{dpv} = (8/n\pi)\sin(n\pi/36)\sin(18n\pi/36) \\ \cdot[\cos(4n\pi/36) + 0.5] \tag{23}$$

For 36-slot/34-pole BLDC motor. In Eqs. (22) and (23), $F_v(r)$ and $G_v(r)$ are functions dependent on radius and harmonic order and are given by Eqs. (24) and (25). i_a, i_b and i_c are three phase winding currents that in a BLDC motor can be expressed as a Fourier series and given by Eq. (26).

$$F_v = \delta v r^{-1}(r/R_s)^v \cdot (1 + (R_r/r)^{2v})/(1 - (R_r/R_s)^{2v}) \tag{24}$$

$$G_v = \delta v r^{-1}(r/R_s)^v \cdot (1 - (R_r/r)^{2v})/(1 - (R_r/R_s)^{2v}) \tag{25}$$

$$i_a = \sum_{n=1}^{\infty}I_n\sin(u(p\omega_r t)) \\ i_b = \sum_{n=1}^{\infty}I_n\sin(u(p\omega_r t - (2\pi/3))) \\ i_c = \sum_{n=1}^{\infty}I_n\sin(u(p\omega_r t - (4\pi/3))) \tag{26}$$

3.3. Unbalanced magnetic force

UMF is the resultant force that acts on rotor due to asymmetric magnetic field. According to Maxwell stress tensor, radial and tangential components of force density

are given by Eqs. (27) and (28) [26].

$$F_r = \left(B_r{}^2 - B_\alpha{}^2\right)/2\mu_0 \qquad (27)$$

$$F_\alpha = \left(B_r B_\alpha\right)/\mu_0 \qquad (28)$$

X and y components of UMF that act on the rotor are F_x and F_y which are as follow:

$$F_x = 0.5 r l_a \mu_0{}^{-1} \int_0^{2\pi} \left[\left(B_\alpha^2 - B_r^2\right)\cos\alpha + 2B_r B_\alpha \sin\alpha\right] d\alpha \quad (29)$$

$$F_y = 0.5 r l_a \mu_0{}^{-1} \int_0^{2\pi} \left[\left(B_\alpha^2 - B_r^2\right)\sin\alpha - 2B_r B_\alpha \cos\alpha\right] d\alpha \quad (30)$$

Where r is the radius in the middle of air-gap, B_r and B_a are radial and tangential flux density and l_a is effective axial length of rotor.

4. FINITE ELEMENT METHOD AND VALIDATION

4.1. 33-slot/34-pole

In machines with $2p = N_s + 1$, the difference between the pole and slot number is one. Since the least common multiple between the pole and slot number is large, the cogging torque is very small; whereas their greatest common divisor is one. Such machines have diametrically asymmetric disposition of stator slots and coils which produce an asymmetric magnetic field and thus the UMFs are generated. Fig. 2 shows winding disposition and flux lines of permanent magnet, armature reaction and resultant fields in 33-slot/34-pole BLDC motor. According to Fig. 2(a), winding is double-layer and each phase of motor includes eleven coils connected in series. According to Fig. 2(b), permanent magnet field is asymmetric especially inside of stator and this is because the number of slots is odd. Therefore the field becomes asymmetric. In Fig 2(c), since in BLDC machines at any moment of time two phases of machine are excited, flux density distribution for one of the phases is zero. The armature reaction field is asymmetric about the diameter of machine and consequently the resultant magnetic field shown in Fig. 2(d), is asymmetrical which caused UMFs.

Radial and tangential components of permanent magnet field distribution on the middle of the air-gap for 33-slot/34-pole BLDC motor were shown in Fig. 3. Since the magnets were magnetized radially, maximum and minimum components of field are located in front of N and S poles. Motor has 34 poles thus there are 34 extreme points in Fig. 3(a). Because Magnet pole-arc to pole-pitch ratio $\left(\alpha_p\right)$ is less than one (0.8616) there is small space between poles. Consequently there is a little slope between maximum and minimum values of flux density. In Fig. 3(b) the amounts of field tangential component located in front of poles are equal to zero. Cuts on the Fig. 3(a) are due to stator slots effect.

Radial and tangential components of armature reaction field distribution on the middle of the air-gap for 33-slot/34-pole BLDC motor were shown in Fig. 4. Because $i_c = 0$ its amount is equal to zero in Fig. 4. In fact, because at any moment of time two phase of machines are excited, the amount of flux density for one phase is equal to zero. In Fig. 4(a) since all teeth of stator were wound, the amplitude of flux density is maximum or minimum. It can be seen that a good agreement has been achieved between analytical and finite element method.

Components of UMF were shown in Fig. 5. Because the commutation period of current is 60 electrical-degree, the frequency of forces is equal to six which is related to (B^+A^-), (C^+A^-), (C^+B^-), (A^+B^-), (A^+C^-) and (B^+C^-) currents and shown in Fig. 6. In the calculation of forces by finite element method, the effects of commutation current are considered and the obtained waveforms represent the exact amount of unbalanced magnetic forces in real conditions (not ideal) of the machine operation. As expected, the magnitude of UMF for 33-slot/34-pole BLDC motor is very large and this is because the magnetic fields in this machine are asymmetric and therefore the resultant magnetic field about diameter of machine is asymmetric.

4.2. 36-slot/34-pole

In machines with $2p = N_s + 2$, the magnetic circuit is symmetrical. It causes the magnetic field distribution to become symmetrical and the magnitude of UMF to be very small. Permanent magnet, armature reaction and resultant fields for 36-slot/34-pole BLDC motor are shown in Fig. 7. According to Fig 7(a), winding is one-layer and each phase of machine includes six coils that are connected in series. Unlike 33-slot/34-pole BLDC motor, permanent magnet and armature reaction field are symmetrical about the diameter of machine and the resultant field distribution in the air-gap is symmetrical.

Figures 8 and 9 show radial and tangential flux densities distribution of permanent magnet and armature reaction field in the middle of the air-gap for 36-slot/34-pole BLDC motor. In Fig. 8(a) like 33-slot/34-pole BLDC motor there are 34 extreme points and the cuts on the Fig. 8(a) related to stator slots effect. In Fig. 9(a) since the teeth were wound every other one thus the amplitude of flux density is maximum, minimum or zero. Because

$i_c = 0$ its amount is equal to zero in Fig. 9. In fact, because at any moment of time two phases of machines are excited, the amount of flux density for one phase is equal to zero. It can be seen that a good agreement has been achieved between analytical and finite element method. Components of UMF were shown in Fig. 10. As expected, the magnitude of UMF for 36-slot/34-pole BLDC motor is equal to zero and this is because the magnetic fields are symmetric.

5. THE INFLUENCE OF PHASE ADVANCE ANGLE METHOD ON UNBALANCED MAGNETIC FORCES

One of the region of operation in BLDC motors is constant power operation in which the speed of motor is higher than the rated speed. In speeds higher than the rated speed, operation frequency increase, thus the reactance of phase winding increase. Fig. 11 indicates the torque-speed curve for two operation areas of machine. In constant-power operation, delay is created in phase current and commutation characteristics and the performance of machine is decreased. There are many methods to solve these problems and to improve the performance of machine. One of them is phase advance angle method. In this method the commutation timing occurs before the rated time and the current phase angle is lead. In this section, the influence of phase advance angle method on the UMF is investigated. In this section, in order to investigate the effect of the phase advance angle on the magnitude of UMFs, UMFs are obtained for a 33-slot/34-pole BLDC motor in the presence of phase advance angles. Since amount of phase advance angle can be varied from zero to 60 degrees, the angles 5, 10, 15, 20, 25, 30, 35, 40, 45, 50 and 55 degrees are selected. In this section, the effect of the commutation of the current in the switching moments is ignored and the current waveform is considered to be ideal. The waveforms obtained from the simulation for the angles are illustrated in Figs. 12-22, respectively. The average amount of UMFs for each phase advance angle value is plotted in Fig. 23. In this figure, the horizontal axis is amount of phase advance angles and the vertical axis is the average value of the UMF for each phase advance angle. By evaluating the results, it is observed that the minimum of UMFs is for angles of 5, 25 and 45 degrees and the maximum of UMFs is for angles of 15, 35 and 55 degrees. It should be noted that by glimpsing at the Fig. 23, We can conclude that for the machine under investigation the maximum and minimum values of UMFs occur approximately at angles with difference of 10 degrees (e.g., the 5 and 15 degrees, which are the minimum and maximum points, have a difference of 10 degrees).

6. CONCLUSION

The UMF is an important factor for the design of the machines that have a fractional ratio of slot number to pole number. In this paper an analytical method for calculation of UMF has been presented and this model has been validated by 2-D finite element analysis and a good agreement obtained between them. Fig. 2. Indicates that whereas the open-circuit flux distribution in the stator core is fairly nonuniform, the air-gap field distribution is more or less symmetrically distributed about the diameter of the machine, although, a slight asymmetry exists due to the odd number of stator slots, which leads to a small unbalanced magnetic force acting on the rotor even on an open circuit. However, the armature reaction field distribution is much more nonuniform, and the resultant air-gap field distribution is correspondingly more asymmetrical. In Fig. 3 flux distribution in all parts of the machines is symmetrical and as a result there is no UMF.

Results show that machine with 33-slot/34-pole has significantly great UMF but in machine with 36-slot/34-pole the magnitude of UMF is equal to zero and this is due to diametrically asymmetric and symmetric distribution of the stator slots and windings. In general:

If the difference between the pole and slot number is one (like 33-slot/34-pole), since the number of poles is even, the number of slots is odd that creates an asymmetric magnetic field and UMF. If the difference between the pole and slot number is equal to two (like 36-slot/34-pole), there are two following modes. If the winding is single-layer, therefore the coil number is half of the slot number. While the number of coils is odd, the machine has diametrically asymmetric disposition of stator slots and phase winding, therefore the resultant UMF is not equal to zero and creates large UMF. If the winding is double-layer, the coil number is equal to the slot number and because the slot number is surely even, the machine has diametrically symmetric disposition of stator slots and phase winding, therefore the resultant UMF is equal to zero.

Also, due to increasing or decreasing of the magnitude of UMF in presence of different phase advance angles, we can conclude that to determine the appropriate phase advance angle, the magnitude of the UMF must be noted and therefore the magnitude of UMF is an important feature in selection of phase advance angle. Notice that combination of UMF and phase advance angles that were investigated in this paper for the first time can be a starting point for next research.

(a)

(b)

(c)

(d)
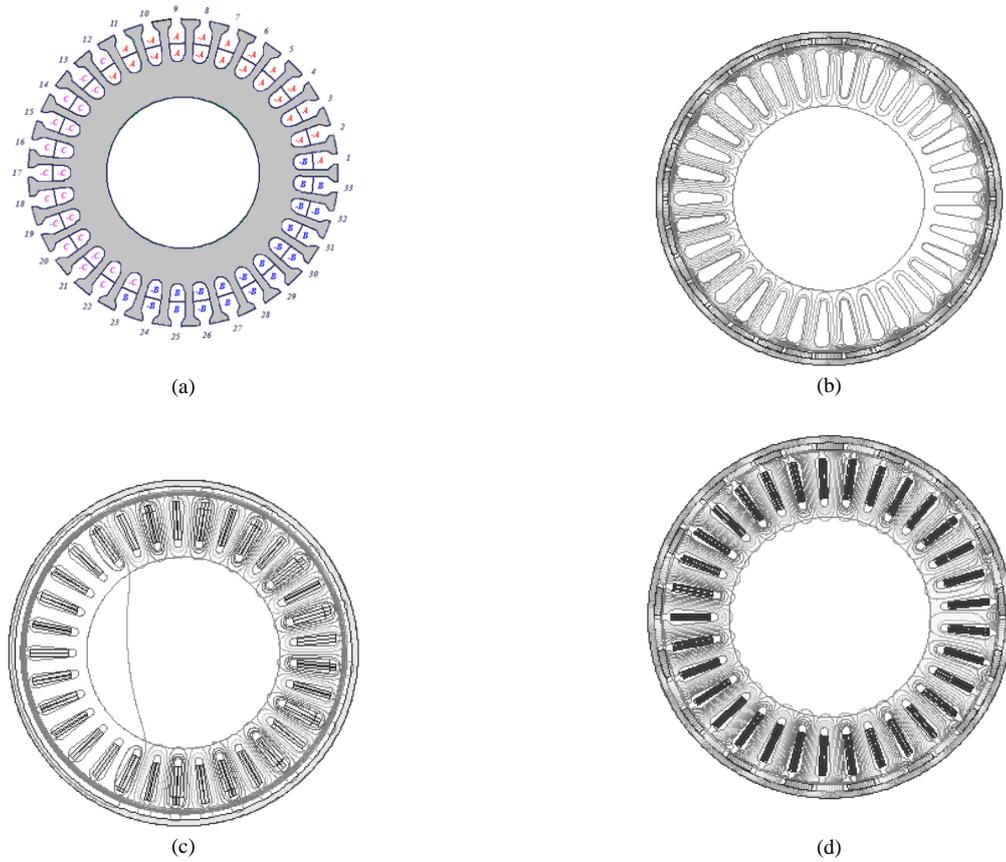
Fig. 2. Disposition of phase winding and display of flux lines in 33-slot/34-pole BLDC motor ($i_a = +79.44\,A$, $i_b = -79.44\,A$ and $i_c = 0$). (a) Winding disposition. (b) Open circuit. (c) Armature reaction. (d) Resultant.

(a)

(b)
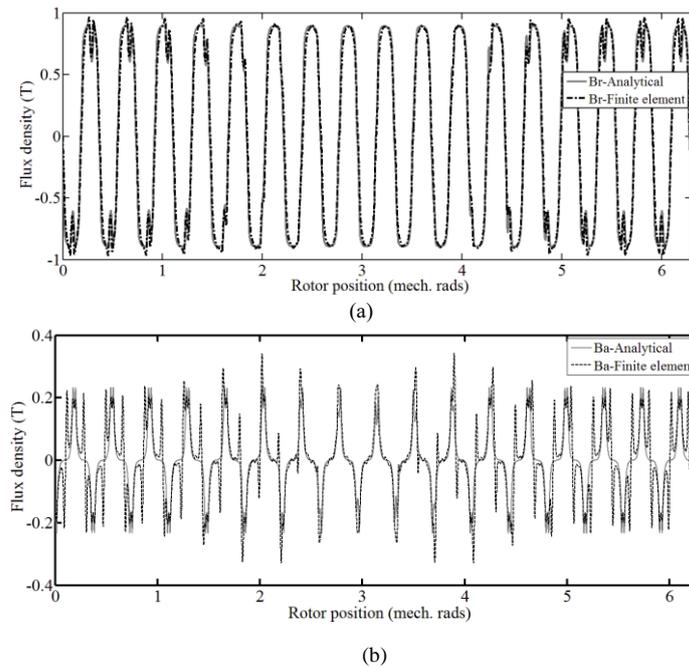
Fig. 3. Permanent magnet field distribution on the middle of the air-gap for 33-slot/34-pole BLDC motor. (a) Radial (b). Tangential.
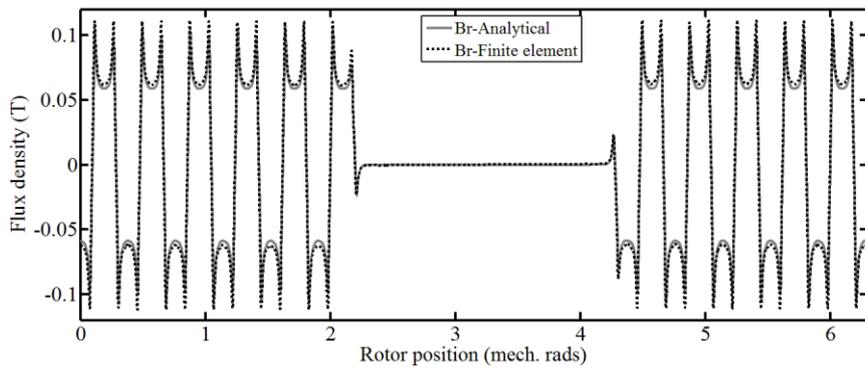
(a)
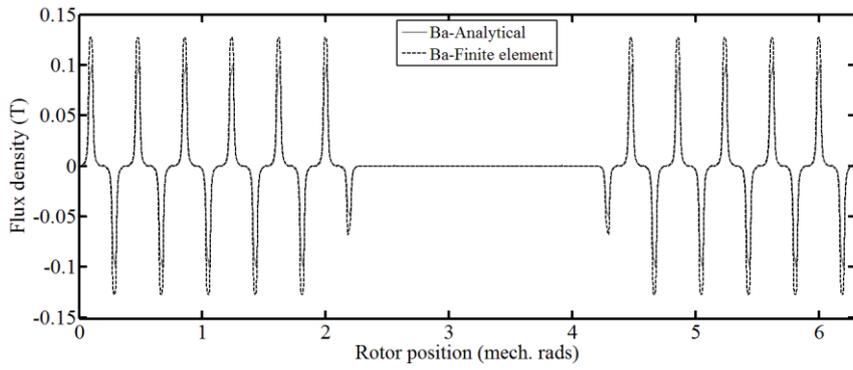
(b)

Fig. 4. Armature reaction field distribution on the middle of the air-gap for 33-slot/34-pole BLDC motor. ($i_a = +79.44$, $i_b = -79.44$ and $i_c = 0$). (a) Radial (b). Tangential
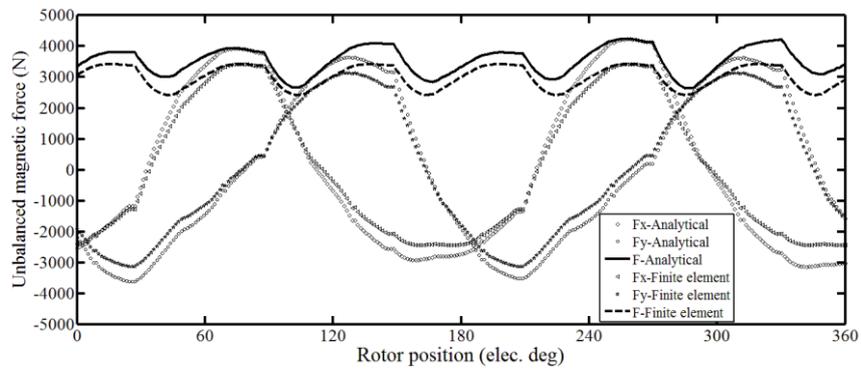
Fig. 5. UMF in the 33-slot/34-pole BLDC motor
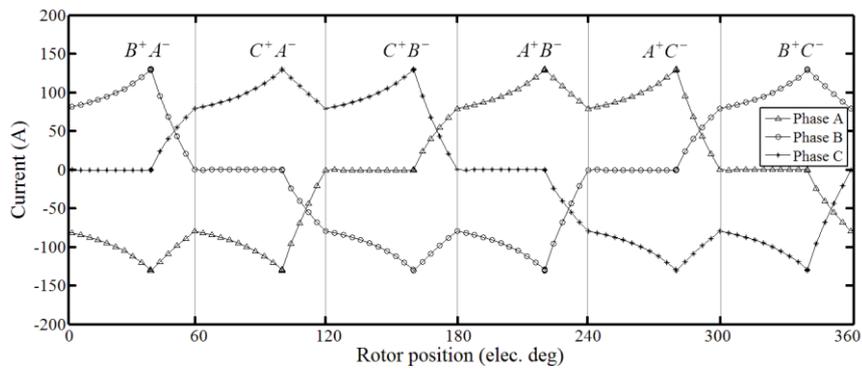
Fig. 6. Phase winding currents for 33-slot/34-pole BLDC motor

(a)

(b)

(c)

(d)
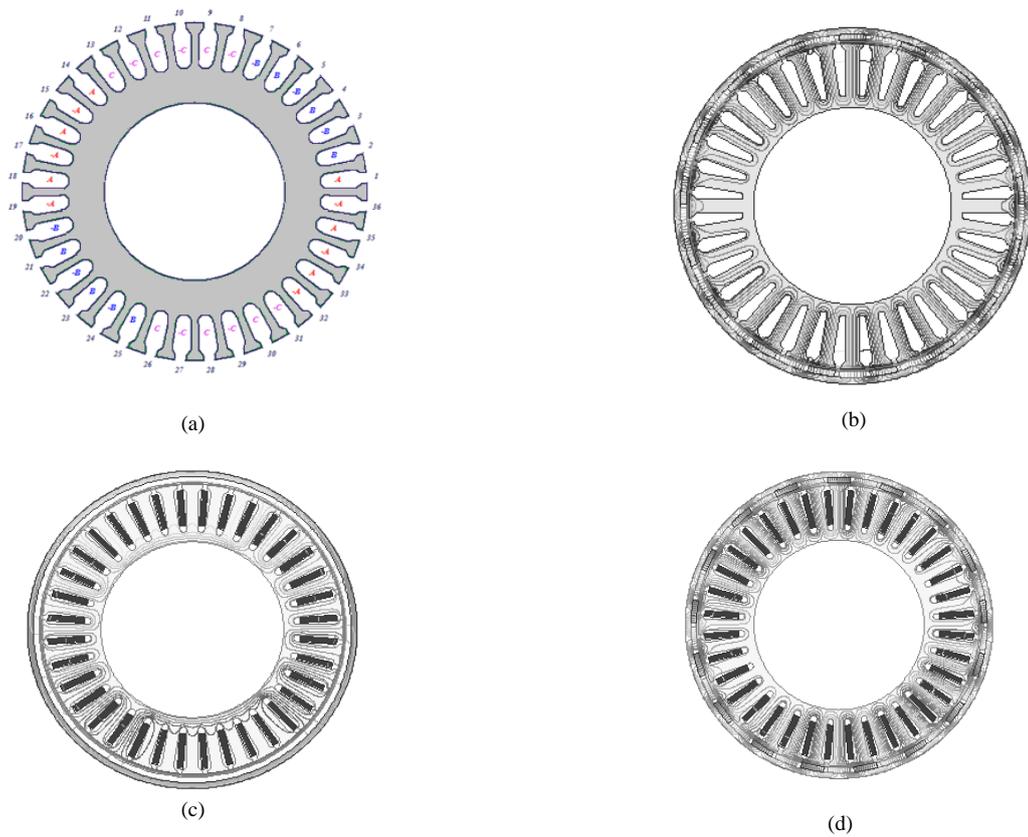
Fig. 7. Disposition of phase winding and display of flux lines in 36-slot/34-pole BLDC motor ($i_a = +79.44$, $i_b = -79.44$ and $i_c = 0$). (a) Winding disposition. (b) Open circuit. (c) Armature reaction. (d) Resultant.

(a)

(b)
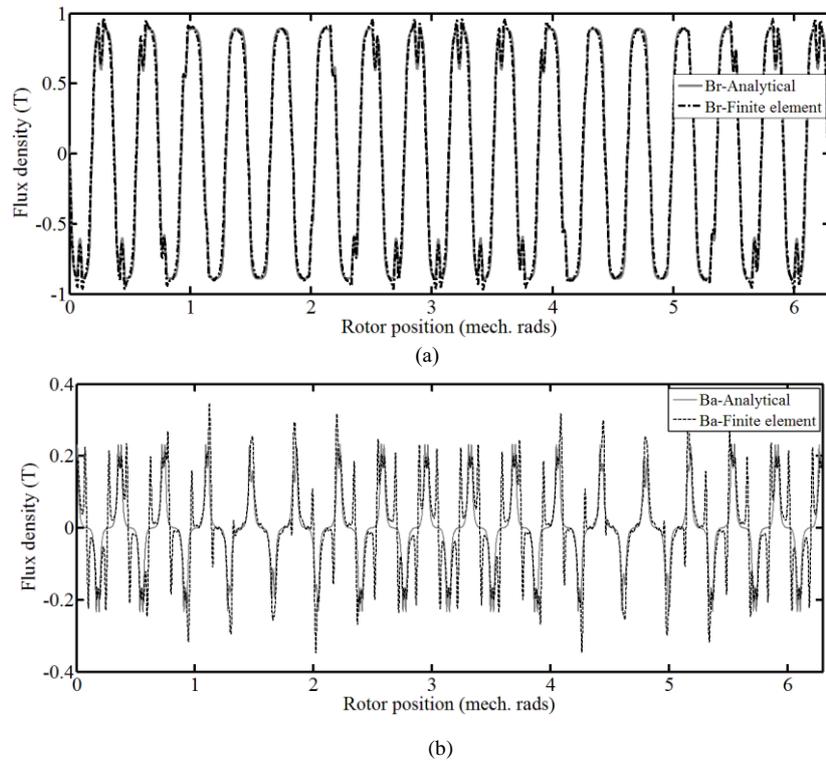
Fig. 8. Permanent magnet field distribution on the middle of the air-gap for 36-slot/34-pole BLDC motor. (a) Radial, (b) Tangential.
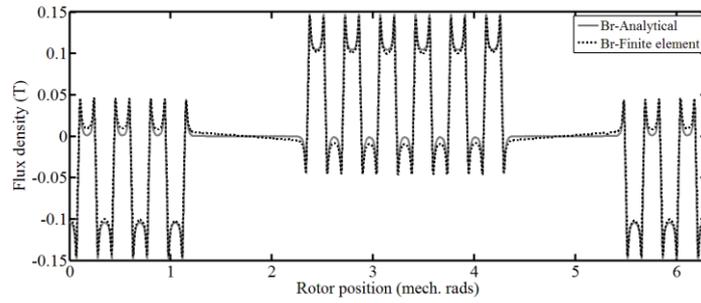
(a)
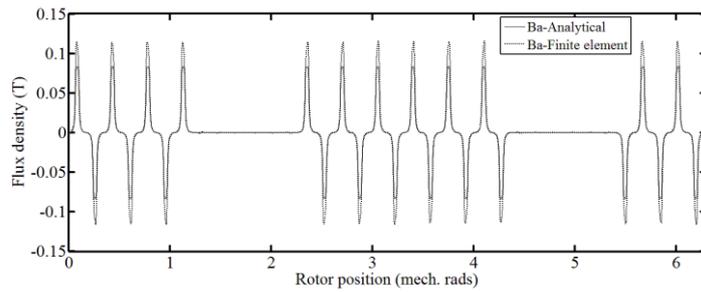
(b)

Fig. 9. Armature reaction field distribution on the middle of the air-gap for 36-slot/34-pole BLDC motor. ($i_a = +79.44$, $i_b = -79.44$ and $i_c = 0$). (a) Radial, (b) Tangential.
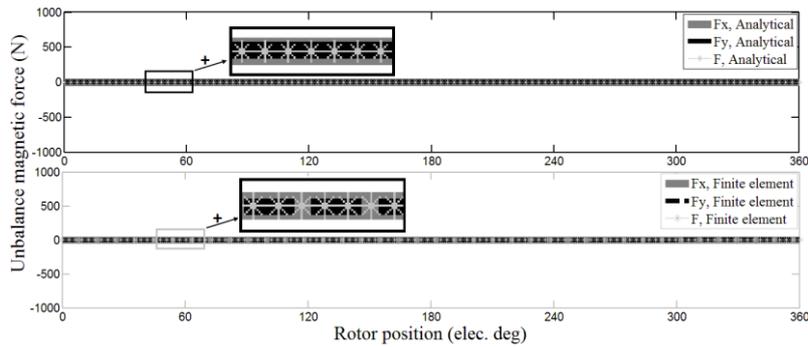
Fig. 10. UMF in the 36-slot/34-pole BLDC motor.
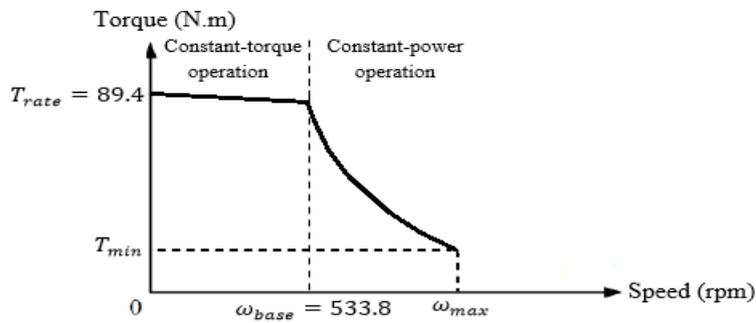
Fig. 11. Torque-speed curves.
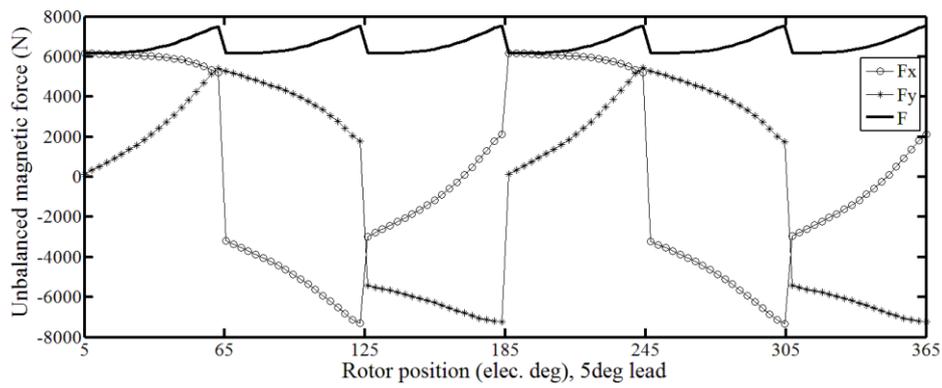
Fig. 12. X, y and resultant components of UMF in the 33-slot/34-pole BLDC motor in presence of 5 degrees of phase advance angle.
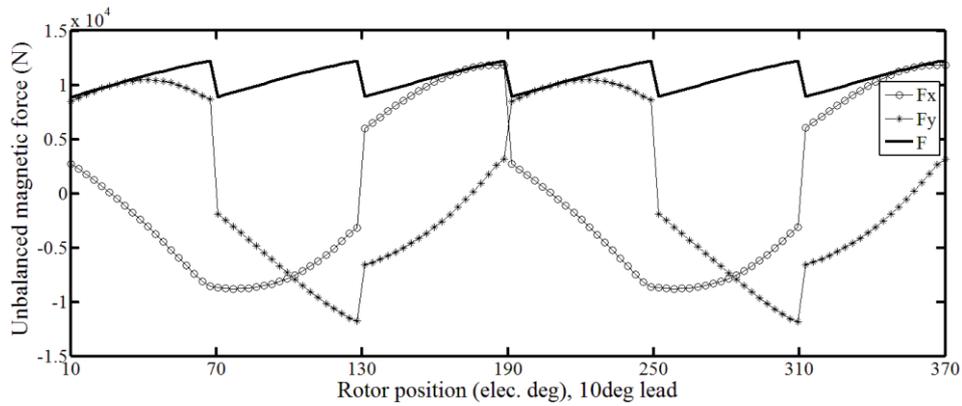
Fig. 13. X, y and resultant components of UMF in the 33-slot/34-pole BLDC motor in presence of 10 degrees of phase advance angle.
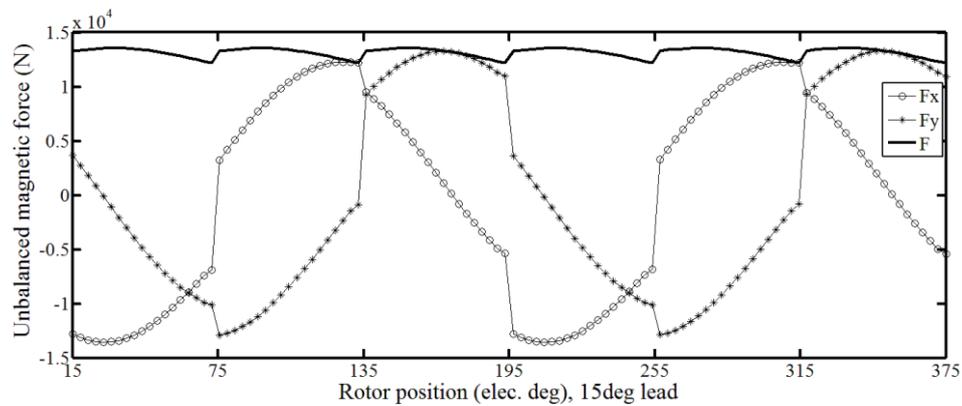
Fig. 14. X, y and resultant components of UMF in the 33-slot/34-pole BLDC motor in presence of 15 degrees of phase advance angle.
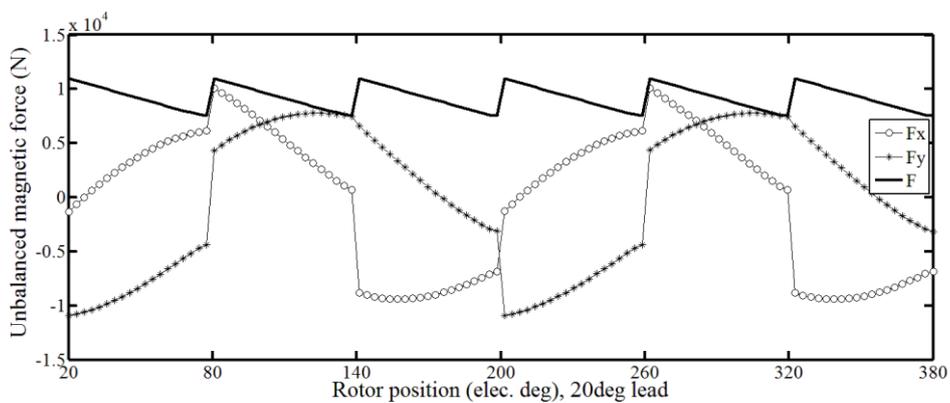
Fig. 15. X, y and resultant components of UMF in the 33-slot/34-pole BLDC motor in presence of 20 degrees of phase advance angle.
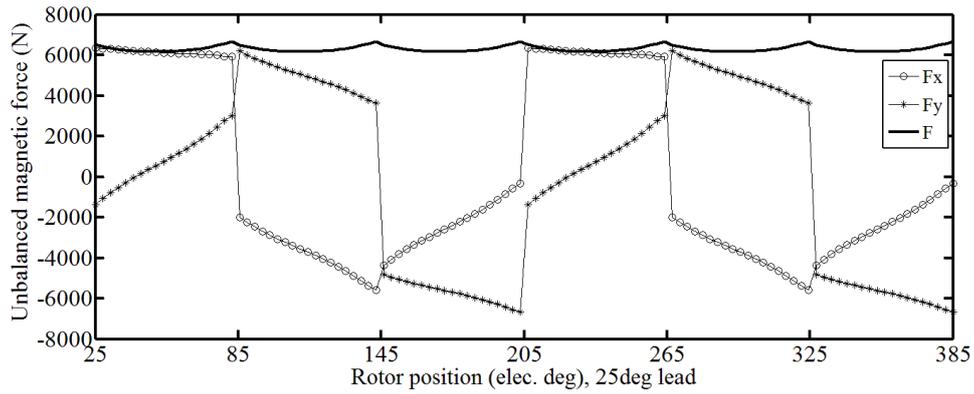
Fig. 16. X, y and resultant components of UMF in the 33-slot/34-pole BLDC motor in presence of 25 degrees of phase advance angle.
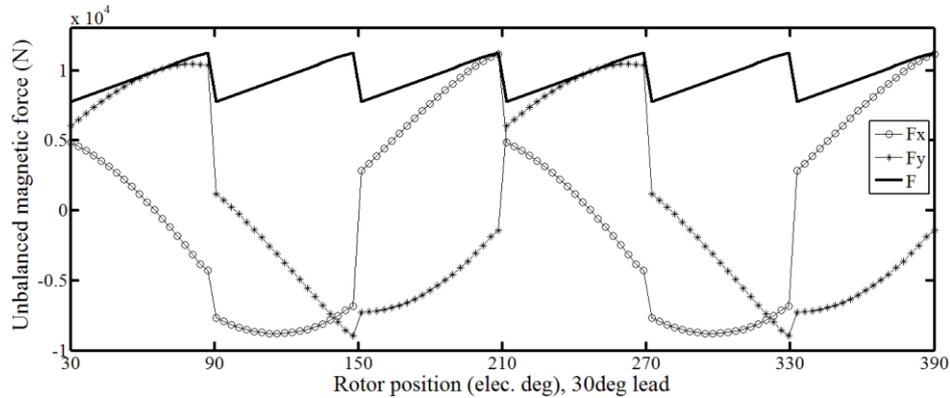
Fig. 17. X, y and resultant components of UMF in the 33-slot/34-pole BLDC motor in presence of 30 degrees of phase advance angle.
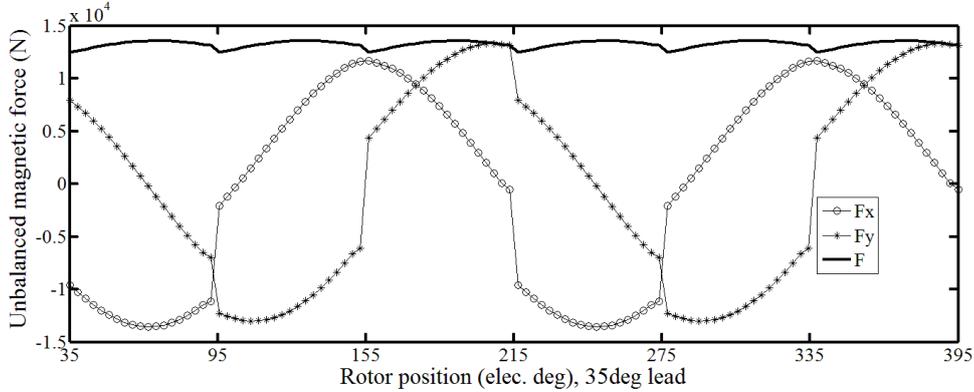
Fig. 18. X, y and resultant components of UMF in the 33-slot/34-pole BLDC motor in presence of 35 degrees of phase advance angle.
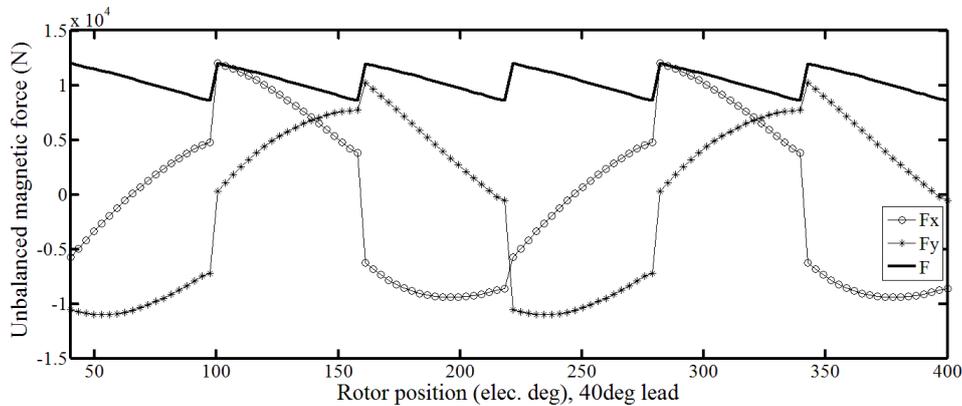
Fig. 19. X, y and resultant components of UMF in the 33-slot/34-pole BLDC motor in presence of 40 degrees of phase advance angle.
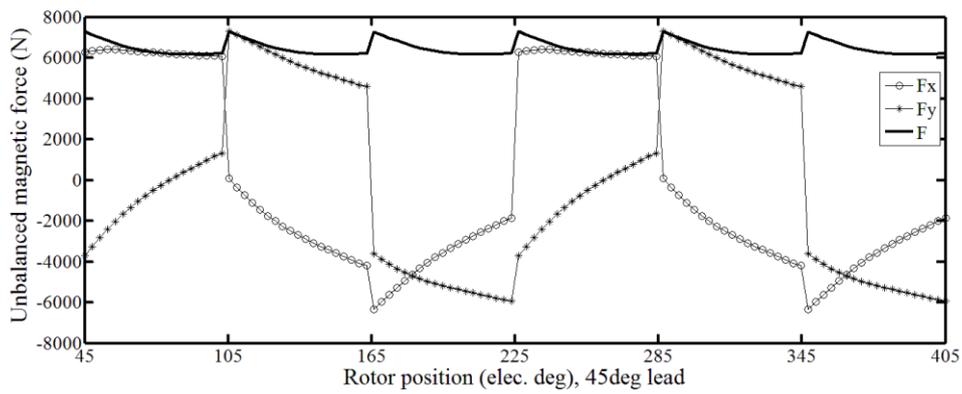
Fig. 20. X, y and resultant components of UMF in the 33-slot/34-pole BLDC motor in presence of 45 degrees of phase advance angle.
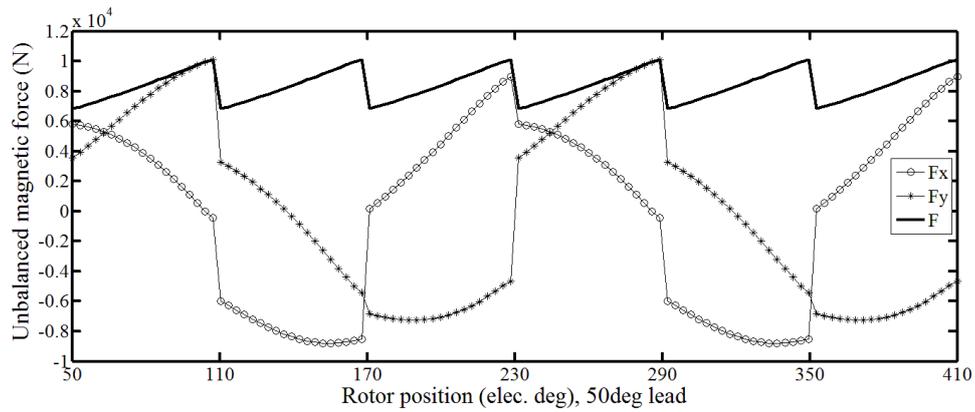
Fig. 21. X, y and resultant components of UMF in the 33-slot/34-pole BLDC motor in presence of 50 degrees of phase advance angle**.**
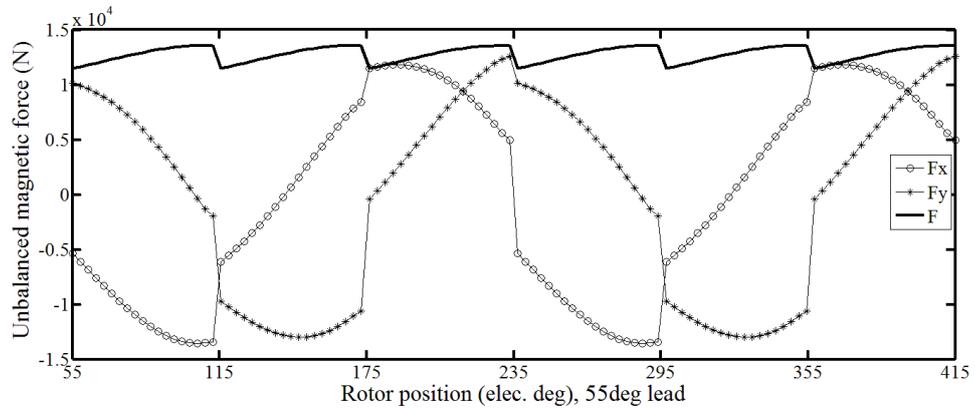
Fig. 22. X, y and resultant components of UMF in the 33-slot/34-pole BLDC motor in presence of 55 degrees of phase advance angle.
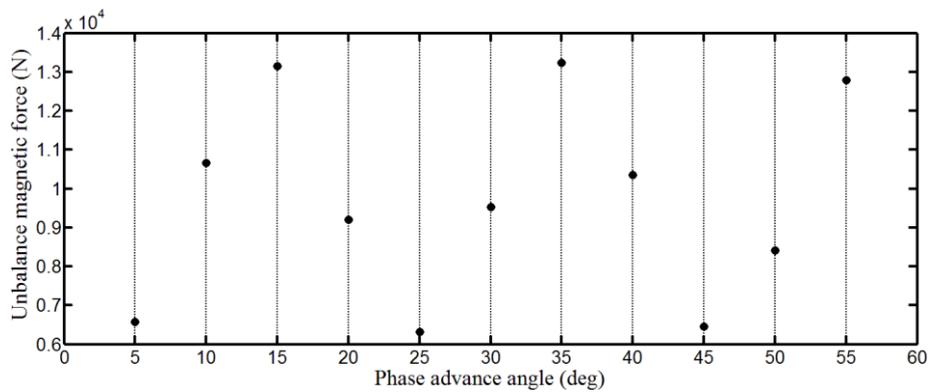
Fig. 23. Average amount of UMFs for each phase advance angle value in the 33-slot/34-pole BLDC machine.

REFERENCES

[1] M. Bigdeli, D. Azizian and E. Rahimpour, "An improved big bang-big crunch algorithm for estimating three-phase induction motors efficiency," *J. Oper. Autom. Power Eng.*, vol. 4, no. 1, pp. 83-92, 2016.

[2] Z. Q. Zhu and D. Howe, "Electrical machines and drives for electric, hybrid, and fuel cell vehicles," in Proce. of the *IEEE*, 2007, pp. 746-765.

[3] A. M. El-Refaie. "Fractional-slot concentrated-windings synchronous permanent magnet machines: Opportunities and challenges," *IEEE Trans. Ind. Electron.*, vol. 57, no. 1, pp. 107-121, 2010.

[4] M. S. Islam, S. Mir and T. Sebastian, "Issues in reducing the cogging torque of mass-produced permanent-magnet brushless DC motor," *IEEE Trans. Ind. Appl.*, vol. 40, no. 3, pp. 813-820, 2004.

[5] N. Bianchi and S. Bolognani, "Design techniques for reducing the cogging torque in surface-mounted PM motors," *IEEE Trans. Ind. Appl.*, vol. 38, no. 5, pp. 1259-1265, 2002.

[6] A. M. El-Refaie and T. M. Jahns, "Optimal flux weakening in surface PM machines using fractional-slot concentrated windings," *IEEE Trans. Ind. Appl.*, vol. 41, no. 3, pp. 790-800, 2005.

[7] A. G. Jack, B. C. Mecrow, P. G. Dickinson, D. Stephenson, J. S. Burdess, N. Fawcett and J. T. Evans, "Permanent-magnet machines with powdered iron cores and prepressed windings," *IEEE Trans. Ind. Appl.*, vol. 36, no. 4, pp. 1077-1084, 2000.

[8] D. Ishak, Z. Q. Zhu and D. Howe, "Permanent magnet brushless machines with unequal tooth widths and similar slot and pole numbers," *IEEE Trans. Ind. Appl.*, vol. 41, no. 2, pp. 584-590, 2005.

[9] D. Ishak, Z. Q. Zhu and D. Howe, "Eddy-current loss in the rotor magnets of permanent-magnet brushless machines having a fractional number of slots per pole," *IEEE Trans. Magn.*, vol. 41, no. 9, pp. 2462-2, 2469, 2005.

[10] D. Ishak, Z. Q. Zhu and D. Howe, "Comparison of PM brushless motors, having either all teeth or alternate teeth wound," *IEEE Trans. Energy Convers.*, vol. 21, no. 1, pp. 95-103, 2006.

[11] R. Wrobel, and P. H. Mellor, "Design considerations of a direct drive brushless machine with concentrated windings," *IEEE Trans. Energy Convers.*, vol. 23, no. 1, pp. 1-8, 2008.

[12] Z. Q. Zhu, Z. P. Xia, L. J. Wu and G. W. Jewell, "Analytical modeling and finite-element computation of radial vibration force in fractional-slot permanent-magnet brushless machines," *IEEE Trans. Ind. Appl.*, vol. 46, no. 5, pp. 1908-1918, 2010.

[13] S. G. Min and B. Sarlioglu, "Modeling and investigation on electromagnetic noise in pm motors with single and double layer concentrated winding for EV and HEV Application," *IEEE Trans. Transp. Electrif.*, vol. 4, no. 1, pp. 292-302, 2018.

[14] Z. Q. Zhu, M. M. Jamil and L. J. Wu, "Influence of slot and pole number combinations on unbalanced magnetic force in PM machines with diametrically asymmetric windings," *IEEE Trans. Ind. Appl.*, vol. 49, no. 1, pp. 19-30, 2013.

[15] Y. Donmezer and L. T. Ergene, "Cogging torque analysis of interior-type permanent-magnet brushless DC motor used in washers," Proce. *8th Int. Symp. Adv. Electromech. Motion Syst. Electr. Drives*, 2009, pp. 1-6.

[16] T. Yoon, "Magnetically induced vibration in a permanent-magnet brushless DC motor with symmetric pole-slot configuration," *IEEE Trans. Magn.*, vol. 41, no. 6, pp. 2173-2179, 2005.

[17] A. Rahideh and T. Korakianitis, "Analytical open-circuit magnetic field distribution of Slotless brushless permanent-magnet machines with rotor eccentricity," *IEEE Trans. Magn.*, vol. 47, no. 12, pp. 4791-2011, 2005.

[18] C. H. Kang, K. J. Kang, J. Y. Song, Y. J. Cho and G. H. Jang, "Axial unbalanced magnetic force in a permanent magnet motor due to a skewed magnet and rotor eccentricities," *IEEE Trans. Magn.*, vol. 53, no. 11, pp. 1-5, 2017.

[19] H. Nazari and N. Rostami, "Diagnosis of different types of air-gap eccentricity fault in switched reluctance motors using transient finite element method," *J. Oper. Autom. Power Eng.*, vol. 3, no. 2, pp. 94-101, 2015.

[20] S. H. Won, W. H. Kim and J. Lee, "Effect of the incomplete magnetization of permanent magnet in the characteristics of BLDC motor," *IEEE Trans. Magn.*, vol. 45, no. 6, pp. 2847-2850, 2009.

[21] G. H. Jang, J. W. Yoon, N. Y. Park and S. M. Jang, "Torque and unbalanced magnetic force in a rotational asymmetric brushless DC motors," *IEEE Trans. Magn.*, vol. 32, no. 5, pp. 5157-5159, 1996.

[22] J. Cros and P. Viarouge, "Synthesis of high performance PM motors with concentrated windings," *IEEE Trans. Energy Convers.*, vol. 17, no. 2, pp. 248-253, 2002.

[23] Z. Q. Zhu, "Fractional slot permanent magnet brushless machines and drives for electric and hybrid propulsion systems" *J. Comput. Math. Electr. Electron. Eng.,* vol. 30, no. 1, pp. 9-31, 2011.

[24] C. C. Chan, J. Z. Jiang, W. Xia and K. T. Chan, "Novel wide range speed control of permanent magnet brushless motor drives," *IEEE Trans. Power Electron.*, vol. 10, no. 5, pp. 539-546, 1995.

[25] S. I. Park, T. S. Kim, S. C. Ahn and D. S. Hyun, "An improved current control method for torque improvement of high-speed BLDC motor," Proce. 8th *Annu. IEEE Appl. Power Electron. Conf.*, 2003, pp. 294-299.

[26] Z. Q. Zhu, D. Ishak, D. Howe and J. Chen, "Unbalanced magnetic forces in permanent-magnet brushless machines with diametrically asymmetric phase windings," *IEEE Trans. Ind. Appl.*, vol. 43, no. 6, pp. 1544-1553, 2007.

[27] Z. Q. Zhu, D. Howe and C. C. Chan, "Improved analytical model for predicting the magnetic field distribution in brushless permanent-magnet machines," *IEEE Trans. Magn.*, vol. 38, no. 1, pp. 229-238, 2002.

[28] Z. Q. Zhu and D. Howe, "Instantaneous magnetic field distribution in brushless permanent magnet DC motors. III. Effect of stator slotting," *IEEE Trans. Magn.*, vol. 29, no. 1, pp. 143-151, 1993.

[29] Z. Q. Zhu and D. Howe, "Instantaneous magnetic field distribution in permanent magnet brushless DC motors. IV. Magnetic field on load," *IEEE Trans. Magn.*, vol. 29, no. 1, pp. 152-158, 1993.

[30] Z. Q. Zhu and D. Howe, "Instantaneous magnetic field distribution in brushless permanent magnet DC motors. II. Armature-reaction field," *IEEE Trans. Magn.*, vol. 29, no. 1, pp. 136-142, 1993.

[31] F. Magnussen and C. Sadarangani, "Winding factors and Joule losses of permanent magnet machines with concentrated windings," Proce. *IEEE Int. Electr. Mach. Drive Conf.*, 2003, pp. 333-339.